Flexural-gravity wave motion in the presence of shear current: Wave blocking and negative energy waves

Santu Das, Prakash Kar, Trilochan Sahoo, and Michael H. Meylan

Citation: Physics of Fluids **30**, 106606 (2018); doi: 10.1063/1.5052228
View online: https://doi.org/10.1063/1.5052228
View Table of Contents: http://aip.scitation.org/toc/phf/30/10
Published by the American Institute of Physics

Flexural-gravity wave motion in the presence of shear current: Wave blocking and negative energy waves

Santu Das,[1,a)] Prakash Kar,[2,b)] Trilochan Sahoo,[2,c)] and Michael H. Meylan[3,d)]
[1]*Department of Mathematics, Indian Institute of Information Technology Bhagalpur, Bhagalpur 813210, India*
[2]*Department of Ocean Engineering and Naval Architecture, Indian Institute of Technology Kharagpur, Kharagpur 721302, India*
[3]*School of Mathematical and Physical Sciences, University of Newcastle, Newcastle, NSW 2308, Australia*

(Received 15 August 2018; accepted 2 October 2018; published online 22 October 2018)

Flexural-gravity wave propagation under the action of a compressive force and in the presence of flow vorticity is studied under the framework of linear water wave theory. The occurrences of wave blocking which is analogous to the free surface gravity wave propagation against an opposing current as well as light wave propagation in curved space-time near a black hole are shown to exist. Moreover, negative energy waves that are responsible for making the total energy of the fluid flow less than that without the waves are also analyzed. The effects of compressive force, Froude number, and vorticity on the existence of negative energy waves as well as the occurrence of flexural-gravity wave blocking are graphically illustrated. The variation in group velocity for different flow parameters such as the vorticity, the Froude number, and the compressive force is analyzed. Time-dependent simulations of the propagation of wave packets are calculated. *Published by AIP Publishing.*
https://doi.org/10.1063/1.5052228

I. INTRODUCTION

The interaction of surface gravity waves with a current has many significant effects. It alters the direction of littoral transport in the coastal region,[1] provides significant resistance to the motion of ships,[2] and affects the construction and installation of marine facilities.[3] Wave-current interaction is a highly complex phenomenon. Ocean currents are generated by wind stress, tidal energy, river flows, bottom friction, etc. In actuality, these currents are often non-uniform along all degrees of freedom and this creates a variation in current speed with depth, characterized by the flow vorticity, which controls the shear flow. This multifaceted interaction between waves and currents can reduce waves, e.g., blocking,[4] or increase them, e.g., freak waves,[5] the reason being the total amount of hydrodynamic energy that is being carried by the waves. A strong example of such interaction is the occurrence of abnormally high amplitude waves near South Africa due to the Agulhas current. This current, which has a maximum surface speed of 2 m/s, interacts with the fully developed ocean waves of height 6 m and results in giant waves of height as high as 18 m or more with a velocity of 10 m/s (see Ref. 5). These waves are potential threats to even large ships.

The concept of wave energy, wave propagation, and wave generation in a medium having shear flow is complex. In some situations, the total hydrodynamic wave energy may change sign to become negative and thus creates the so-called negative energy wave (NEW) (see Refs. 6–8). The physical explanation of NEW is that the total hydrodynamic energy of the medium with the wave is less than that of the medium without the wave. Consequently, no energy is required to generate NEW, instead energy can be extracted from the system by exciting NEW. Apart from hydrodynamic shear flows, such NEW exists in plasma physics and electronics (see Refs. 9–11). Furthermore, the occurrence of NEW allowed hydrodynamic instabilities, such as the Kelvin-Helmholtz instability, to be interpreted in terms of the energy transfer between positive energy waves and NEW.[11] The surface wave energy of capillary-gravity waves was determined in the presence of a shear flow with a linear velocity profile.[12] However, the possible occurrence of NEW was overlooked and not derived until Maïssa, Rousseaux, and Stepanyants.[8] Recently, the existence of waves with negative kinetic energy (but not NEW) for a floating elastic plate in the presence of a compressive force and an opposing uniform current (no shear flow) was shown to exist.[13] This study was extended to two-layered fluid,[14] taking into account the effect of a density ratio but without a current.

An opposing current often acts as a breakwater as it can attenuate propagating wave energy and reduce the wave height in the direction of propagation.[15] The interaction of gravity waves and the opposing current blueshifts the waves, i.e., shortens the wavelength and reduces the group velocity. The group velocity can even vanish for a sufficiently high opposing current, known as wave blocking. Near this blocking point, an increase in potential energy is observed due to the gradual increase in the height of the wave. Simultaneously, since the group velocity decreases, the increased potential energy is compensated by a reduction in the kinetic energy. Hence, the wavelength is blue-shifted as the wave approaches the blocking point. Furthermore, waves with relatively small

[a)]Author to whom correspondence should be addressed: santudas20072@gmail.com
[b)]Electronic mail: pkprakash47@gmail.com
[c)]Electronic addresses: tsahoo1967@gmail.com and tsahoo@naval.iitkgp.ac.in
[d)]Electronic mail: mike.meylan@newcastle.edu.au

amplitude can even be reflected near the blocking point (see Ref. 16) acting as a white-hole, which cannot be penetrated. As a result of the energy transfer, the wave environment near the blocking point becomes very rough, causing difficulties in navigation and transiting such regions (which commonly occur in tidal inlet areas). The mathematical analysis of the blocking phenomenon due to the interaction of the opposing current was first described by Peregrine[17] using linear water wave theory. The effect of flow vorticity on surface gravity waves has been studied by many researchers, some of which are discussed here. Dalrymple[18] derived a finite amplitude wave-current interaction model with constant vorticity and proposed the generation of regular and irregular waves analytically. Kirby and Chen[19] derived an approximate dispersion relation for surface gravity waves having vertically sheared flow in the presence of a weak current. With the help of a perturbation technique, it was concluded that a second-order approximation was required to obtain accurate results in finite water depth. Nepf and Monismith[20] carried out an experimental study on surface wave dispersion in a shear current. A shift in wavenumber due to vorticity (apart from Doppler shift) was measured and matched with the dispersion relation provided by Miles.[21] Ellingsen and Brevik[12] studied wave-current interaction in the presence of constant vorticity to show that the average potential and kinetic energies are not equal when the current is non-uniform. However, the effect of surface tension in wave-current interaction problems was introduced by Trulsen and Mei[22] who analytically established the existence of the secondary blocking point. The effect of vorticity was included later.[23] Furthermore, various analytical relations related to wave blocking were established in Ref. 24 along with the particular case of purely capillary waves. Flexural-gravity wave blocking was mathematically established by Das, Sahoo, and Meylan[13] both in the presence of compressive force and with/without the opposing current but in the absence of vorticity.

The objective of this work is to establish the condition for the existence of NEW and blocking for flexural-gravity waves in the presence of linearly varying current with depth. The mathematical problem will be solved for arbitrary water depth, and various results associated with NEW and blocking will be discussed for deep and shallow water approximations. The present work is an extension that of of Das, Sahoo, and Meylan[13] in which we incorporate a vorticity factor and study its effect on the critical compressive forces where blocking initiates as well as buckling occurs. The outline of the paper is as follows. A mathematical formulation is provided in Sec. II. It includes total wave energy derivation, NEW, and blocking criteria for both shallow and deep water. Numerical results pertaining to NEW and wave blocking are detailed in Sec. III. Section IV contains some time-domain simulations in support of the theoretical findings, and the paper ends with a brief conclusion in Sec. V.

II. MATHEMATICAL FORMULATION

The physical problem is formulated in a two-dimensional Cartesian co-ordinate system (x, z) with z- and x-axes being the vertically upward and horizontal directions, respectively. An infinitely extended fluid domain along the x-axis, occupying the region $-\infty < x < \infty$, $-h < z < 0$ of finite depth h is considered for the study. Note that we will consider the limit as the depth goes to infinity as a special case in what follows. An ice sheet, modeled as a thin elastic plate of uniform thickness d and flexural rigidity EI acting under uniform compressive force N, is assumed to be freely floating on top of the fluid domain. Furthermore, the background fluid velocity is assumed to be a linear function of the vertical depth. The horizontal component of the velocity is defined as $u(x, z) = U_0 + \alpha z$ with U_0 being the fluid speed at the ice-covered fluid surface and α being a constant, which characterizes the background flow vorticity. We assume that the vertical component of the velocity is zero.

Without loss of generality, it is assumed that U_0 is co-directed with the positive x-axis, i.e., $U_0 > 0$. Following Maïssa, Rousseaux, and Stepanyants,[8] we note that if we write the Euler equation in the Helmholtz form, we get

$$\frac{\partial(\text{curl } \mathbf{v})}{\partial t} = (\text{curl } \mathbf{v} \cdot \nabla)\mathbf{v} - (\mathbf{v} \cdot \nabla)\text{curl } \mathbf{v}. \tag{1}$$

Then, we can write the velocity as $\mathbf{v} = \tilde{\mathbf{v}} + u\mathbf{i}$, where $\mathbf{i}$ is the unit vector in the x direction, to get

$$\frac{\partial(\text{curl } \tilde{\mathbf{v}})}{\partial t} = -(\mathbf{v} \cdot \nabla)(\text{curl } \tilde{\mathbf{v}} - \text{curl } u\mathbf{i}). \tag{2}$$

We note that curl $u\mathbf{i}$ is constant and hence $\mathbf{v} \cdot \nabla(\text{curl } u\mathbf{i}) = 0$ which means that if $\tilde{\mathbf{v}}$ is irrotational at a given time it will remain irrotational for all time. Note that this is only true for a linear shear flow.[25] Therefore, we assume that the velocity $\mathbf{v}(x, z, t)$ can be written in the form $\mathbf{v}(x, z, t) = u(z)\mathbf{i} + \nabla\phi(x, z, t)$, where $\tilde{\mathbf{v}} = \nabla\phi(x, z, t)$.

The velocity potential $\phi(x, z, t)$ satisfies the following governing equation:

$$\frac{\partial^2\phi}{\partial x^2} + \frac{\partial^2\phi}{\partial z^2} = 0 \quad \text{on} \quad -\infty < x < \infty, -h < z < 0, \tag{3}$$

along with the bottom impermeable condition

$$\frac{\partial\phi}{\partial z} = 0 \quad \text{on} \quad z = -h. \tag{4}$$

If the ice sheet deflection is denoted by $\eta(x, t)$, the linearized kinematic boundary condition on the ice covered surface is given by

$$\frac{\partial\eta}{\partial t} + u\frac{\partial\eta}{\partial x} = \frac{\partial\phi}{\partial z}$$

$$\text{or} \quad \frac{\partial\eta}{\partial t} + U_0\frac{\partial\eta}{\partial x} = \frac{\partial\phi}{\partial z} \quad \text{on} \quad z = 0. \tag{5}$$

Assuming that an in-plane compressive force N acts on the homogeneous floating ice sheet along the x-axis, the ice sheet deflection satisfies the thin plate equation given by (see Refs. 26–30)

$$\left(EI\frac{\partial^4}{\partial x^4} + N\frac{\partial^2}{\partial x^2} - \rho_i d\frac{\partial^2}{\partial t^2}\right)\eta(x, t) = p_s \quad \text{on} \quad z = 0, \tag{6}$$

with p_s being the external force acting on the floating ice sheet and ρ_i being the mass per unit area of the ice sheet. We assume from now on that the elastic restoring force is sufficiently large compared to the inertial force of the elastic plate that we can

ignore the inertial term. This assumption is not essential to what follows but is true in almost all situations where the thin plate model is applicable. Therefore Eq. (6) is rewritten as

$$\left(EI\frac{\partial^4}{\partial x^4}+N\frac{\partial^2}{\partial x^2}\right)\eta(x,t)=p_s \quad \text{on} \quad z=0. \tag{7}$$

To account for the vorticity effect, the following Euler equation in the Lamb form is utilized:

$$\frac{\partial \mathbf{v}}{\partial t}+\nabla\left(\frac{\mathbf{v}^2}{2}+\frac{p_s}{\rho}+gz\right)=\mathbf{v}\times\text{curl}(\mathbf{v}). \tag{8}$$

Since $\mathbf{v}(x,z,t)=u(z)\mathbf{i}+\nabla\phi(x,z,t)$, the x-component of $\mathbf{v}$ is $u(z)+\frac{\partial\phi}{\partial x}$ with $u(z)=U_0+\alpha z$. Similarly, the x-component of $\mathbf{v}^2$ is $2U_0\frac{\partial\phi}{\partial x}$ (ignoring the higher order terms). Hence, the x-component of Eq. (8) becomes

$$\frac{\partial}{\partial t}\left(\frac{\partial\phi}{\partial x}\right)+\frac{\partial}{\partial x}\left(\frac{2U_0\frac{\partial\phi}{\partial x}}{2}+\frac{p_s}{\rho}+gz\right)=-\alpha\left(\frac{\partial\phi}{\partial z}\right). \tag{9}$$

After simplification, the following equation is obtained:

$$\frac{\partial}{\partial x}\left(\frac{\partial\phi}{\partial t}+U_0\frac{\partial\phi}{\partial x}+\frac{p_s}{\rho}+g\eta\right)=-\alpha\frac{\partial\phi}{\partial z} \quad \text{on} \quad z=0. \tag{10}$$

The free surface boundary condition is obtained by eliminating p_s from Eqs. (7) and (10) as

$$\frac{\partial}{\partial x}\left\{\left(\rho\frac{\partial\phi}{\partial t}+\rho U_0\frac{\partial\phi}{\partial x}+\rho\eta\right)+\left(EI\frac{\partial^4}{\partial x^4}+N\frac{\partial^2}{\partial x^2}\right)\eta\right\} = -\rho\alpha\frac{\partial\phi}{\partial z}. \tag{11}$$

Considering periodic motion in time and x-direction, the plane flexural gravity wave profile $\eta(x,t)$ and velocity potential $\phi(x,z,t)$ are taken as

$$\eta(x,t)=Ae^{\{\mathrm{i}(\omega t-kx)\}}, \quad \phi(x,z,t)=B\cosh\{k(z+h)\}e^{\{\mathrm{i}(\omega t-kx)\}}, \tag{12}$$

where A and B are arbitrary constants whose relation can be computed from Eqs. (5) and (12) as

$$B=\mathrm{i}A\frac{\omega-\kappa^{\pm}U_0|k|}{|k|\sinh(|k|h)},$$

where ω is the angular frequency of the flexural gravity wave and $\kappa^{\pm}=\pm1$ for co-propagating and counter-propagating waves, respectively. Both k and U_0 are positive when the wave is co–propagating with the current, but k becomes negative when the wave changes direction. Now the following dispersion relation can be obtained from Eqs. (3), (4), and (10):

$$(\omega-\kappa^{\pm}U_0|k|)^2+\alpha(\omega-\kappa^{\pm}U_0|k|)\tanh(|k|h) -\left(\frac{EI}{\rho}k^4-\frac{N}{\rho}k^2+g\right)|k|\tanh(|k|h)=0,$$

whose positive branch can be represented as

$$\omega=\kappa^{\pm}U_0|k|\left(1-\frac{\alpha}{2}\frac{\tanh(|k|h)}{U_0|k|}\right) +\sqrt{\left(\frac{\alpha}{2}\tanh(|k|h)\right)^2+\left(g-\frac{N}{\rho}k^2+\frac{EI}{\rho}k^4\right)|k|h}. \tag{13}$$

In terms of the normalized variables $\tilde{\omega}=\omega\sqrt{h/g}$, $\tilde{k}=kh$, $\text{Fr}=\frac{U_0}{\sqrt{gh}}$ (Froude number), $\Omega=\frac{\alpha h}{2\sqrt{gh}}$ (normalised vorticity), $D=\frac{EI}{\rho gh^4}$ (normalized flexural rigidity of the plate), $Q=\frac{N}{\rho gh^2}$ (normalized compressive force), the positive branch of the dispersion relation is obtained as

$$\tilde{\omega}^{\pm}_{\oplus}=\kappa^{\pm}(\text{Fr}|\tilde{k}|-\Omega\tanh|\tilde{k}|) +\sqrt{(\Omega\tanh|\tilde{k}|)^2+(D\tilde{k}^4-Q\tilde{k}^2+1)|\tilde{k}|\tanh|\tilde{k}|}. \tag{14}$$

In this dispersion relation, $\tilde{\omega}^{\pm}_{\oplus}$ represents co-propagating and counter-propagating wave frequencies, respectively.

Similarly, the negative branch of the dispersion relation can be represented as

$$\tilde{\omega}^{\pm}_{\ominus}=\kappa^{\pm}(\text{Fr}|\tilde{k}|-\Omega\tanh|\tilde{k}|) -\sqrt{(\Omega\tanh|\tilde{k}|)^2+(D\tilde{k}^4-Q\tilde{k}^2+1)|\tilde{k}|\tanh|\tilde{k}|}. \tag{15}$$

In the subsequent analysis, we will consider only the positive branch of the dispersion relation unless otherwise mentioned. Hence, the subscript $\oplus$ is dropped for simplicity.

A. Wave energy

The potential energy for the plane flexural-gravity wave in the presence of the uniform compressive force N is given by (see Ref. 31)

$$\mathcal{P}=\frac{\rho A^2}{4}\left(g+\frac{EI}{\rho}k^4-\frac{N}{\rho}k^2\right). \tag{16}$$

It is notable that the potential energy does not depend on the flow velocity but entirely on the deflection of the free surface from its equilibrium position. Keeping the parameters ρ, EI, N, A fixed, the potential energy can be considered a function of wavenumber k as $\mathcal{P}=\mathcal{P}(k)$. $\mathcal{P}(k)$ has a minimum at $k=\sqrt{2N/3EI}$ and the corresponding value of $\mathcal{P}(k)=1-2N^2/(9\rho gEI)>0$ as $N^2<4\rho gEI$ (compressive force corresponding to plate buckling). Hence potential energy is always positive. Following Maïssa, Rousseaux, and Stepanyants,[8] the kinetic energy of the wave motion is determined as the time average over a wave period of the difference in the kinetic energy of the moving fluid in the presence of a current with that when the current is absent. Moreover, the wave energy is proportional to the squared wave amplitude under the linear approximation. Under these assumptions, the kinetic energy of the system is represented as

$$\begin{aligned}\mathcal{K}&=\frac{\rho}{2}\left\langle\int_{-h}^{\eta}\left\{[u+U(z)]^2+v^2-[U(z)]^2\right\}\right\rangle,\\ &=\frac{\rho}{2}\left\langle\int_{-h}^{\eta}\left\{u^2+v^2+2u[U(z)]^2\right\}\right\rangle,\\ &\approx\frac{\rho}{2}\left\langle\int_{-h}^{0}\{u^2+v^2\}\right\rangle+\rho\left\langle\int_{-h}^{0}uU(z)\right\rangle+\rho\left\langle\int_{0}^{\eta}uU(z)\right\rangle.\end{aligned} \tag{17}$$

The approximation in the first integrand is feasible due to its quadratic form and positive value. Moreover, the average value of the second integrand will now be zero as it is a periodic function in time. The last integral can be approximated

by $\rho U(0)\langle\eta(x,t)u(x,0,t)\rangle$. Now utilizing the following two relations

$$u(x,z,t) = \mathrm{Re}\left(\frac{\partial\phi}{\partial x}\right) \quad \text{and} \quad v(x,z,t) = \mathrm{Re}\left(\frac{\partial\phi}{\partial z}\right), \tag{18}$$

we obtain the following expression for the kinetic energy from Eq. (17):

$$\mathcal{K} = \frac{\rho^2 A^2}{4}\frac{\omega^2 - U_0^2 k^2}{|k|\tanh(|k|h)}. \tag{19}$$

The kinetic energy for co-propagative waves $\mathcal{K}^+$ and counter-propagative waves $\mathcal{K}^-$ is obtained by using Eqs. (13) and (19) as

$$\mathcal{K}^{\pm} = \frac{\rho A^2}{4}\left\{\left(\frac{EI}{\rho}k^4 - \frac{N}{\rho}k^2 + g\right) + \alpha\left(U_0 - \frac{\alpha}{2}\frac{\tanh(|k|h)}{|k|}\right) \times\left[\kappa^{\pm}\sqrt{1 + 4\left(\frac{EI}{\rho}k^4 - \frac{N}{\rho}k^2 + g\right)\frac{|k|}{\alpha^2\tanh(|k|h)}} - 1\right]\right\}. \tag{20}$$

Furthermore, using the dimensionless form of the variables as in Eq. (14), the ratio of the kinetic and potential energies is expressed as

$$\mathcal{R}^{\pm} = \frac{\mathcal{K}^{\pm}}{\mathcal{P}} = 1 + 2\frac{\Omega}{\left(D|\tilde{k}|^4 - Q|\tilde{k}|^2 + 1\right)}\left(\mathrm{Fr} - \Omega\frac{\tanh|\tilde{k}|}{|\tilde{k}|}\right) \times\left[\left(\kappa^{\pm}\sqrt{1 + \left(D\tilde{k}^4 - Q\tilde{k}^2 + 1\right)\frac{|\tilde{k}|}{\Omega^2\tanh|\tilde{k}|}} - 1\right]. \tag{21}$$

In the absence of vorticity ($\Omega = 0$), the above relation is simplified to

$$\mathcal{R}^{\pm} = \frac{\mathcal{K}^{\pm}}{\mathcal{P}} = 1 + 2\frac{\mathrm{Fr}}{\left(D|\tilde{k}|^4 - Q|\tilde{k}|^2 + 1\right)} \times\left[\kappa^{\pm}\sqrt{\left(D\tilde{k}^4 - Q\tilde{k}^2 + 1\right)\frac{|\tilde{k}|}{\tanh|\tilde{k}|}}\right]. \tag{22}$$

For a counter-propagating wave and sufficiently large Froude number, the energy ratio may become negative. It may be noted that this can occur only when the kinetic energy becomes negative since the potential energy cannot be negative. Thus the condition for the existence of the negative energy wave is obtained from Eq. (22) as

$$\mathrm{Fr} > \frac{\mathrm{Fr}_c}{2}, \text{ where } \mathrm{Fr}_c = \sqrt{\left(D\tilde{k}^4 - Q\tilde{k}^2 + 1\right)\frac{\tanh|\tilde{k}|}{|\tilde{k}|}}. \tag{23}$$

Fr_{min}, the minimum value of the Froude number for the occurrence of negative energy waves, is readily obtained from the following parametric form:

$$D(\tilde{k}) = \frac{|\tilde{k}|(1-\tanh^2\tilde{k})(Q\tilde{k}^2 - 1) + (1 + Q\tilde{k}^2)\tanh\tilde{k}}{|\tilde{k}|^4\left(|\tilde{k}|(1-\tanh^2\tilde{k}) + 3\tanh|\tilde{k}|\right)}, \tag{24}$$

$$\mathrm{Fr}_{min}(\tilde{k}) = \frac{\tanh|\tilde{k}|}{\sqrt{2\tilde{k}}}\sqrt{\frac{(2 - Q\tilde{k}^2)}{|\tilde{k}|(1-\tanh^2|\tilde{k}|) + 3\tanh|\tilde{k}|}}. \tag{25}$$

In particular, if $\alpha = Q/\sqrt{D}$, then

$$\mathrm{Fr}_{min}(\alpha) = \frac{D^{1/8}\sqrt{12 - (\alpha^2 + \sqrt{\alpha^4 + 12\alpha^2})}}{6^{3/4}\left(\alpha + \sqrt{\alpha^2 + 12}\right)^{1/4}}. \tag{26}$$

B. Negative energy waves

Wave energy plays an important role in hydrodynamic shear flows concerning wave generation, propagation, and absorption. One of the important aspects of such wave propagation, based on linear water-wave theory, is the quasi-energy, details of which are provided in the work of Maïssa, Rousseaux, and Stepanyants,[24] of monochromatic waves. Its relation with the total energy of the flow is established in the work of Maïssa, Rousseaux, and Stepanyants.[8] The most striking feature of quasi-energy is the occurrence of negative energy waves (NEWs) characterised by a change in the sign of wave energy to become negative in the presence of shear flow. Surprisingly, in the presence of NEW, the total wave energy of the medium turns out to be less compared to the total energy of the medium without waves. Consequently, no energy is required to generate NEW, instead energy can be extracted from the system by exciting NEW. Hence, the more the energy is extracted from the system, the stronger the NEW can be excited. These concepts are very important in analyzing different types of hydrodynamic instabilities such as dissipative[9] and radiative instabilities.[7] In the presence of an appropriate energy sink, an exponential growth of NEW in time is observed under the linear approximation. This is mainly due to the conversion of the kinetic energy of shear flow into the wave energy of small perturbation (see Refs. 11 and 32). However, the existence of NEW does not necessarily guarantee instabilities. However, the occurrence of such NEW in flexural-gravity waves is not well known. An attempt is made in this work to understand it mathematically and, consequently, study the effect of various hydroelastic parameters on the generation of such waves.

The total period-averaged wave energy is given by

$$E = \mathcal{P} + \mathcal{K}:$$

$$E^{\pm} = \frac{\rho A^2}{2}\left\{\left(\frac{EI}{\rho}k^4 - \frac{N}{\rho}k^2 + g\right) + \frac{\alpha}{2}\left(U_0 - \frac{\alpha}{2}\frac{\tanh(|k|h)}{|k|}\right) \times\left[\kappa^{\pm}\sqrt{1 + 4\left(\frac{EI}{\rho}k^4 - \frac{N}{\rho}k^2 + g\right)\frac{|k|}{\alpha^2\tanh(|k|h)}} - 1\right]\right\}, \tag{27}$$

whose non-dimensional form is obtained as

$$\mathcal{E}^{\pm} = \left\{\left(1 - Q|\tilde{k}|^2 + D|\tilde{k}|^4\right) + \Omega\left(\mathrm{Fr} - \Omega\frac{\tanh|\tilde{k}|}{|\tilde{k}|}\right) \times\left[\kappa^{\pm}\sqrt{1 + \left(D\tilde{k}^4 - Q\tilde{k}^2 + 1\right)\frac{|\tilde{k}|}{\Omega^2\tanh|\tilde{k}|}} - 1\right]\right\}. \tag{28}$$

The expression for the wave energy can also be presented using the dispersion relation as

$$E^{\pm} = \frac{\rho A^2}{2|k|\tanh(|k|h)}(\omega^{\pm} - \kappa^{\pm}U_0|k|)\left[\omega^{\pm} + \kappa^{\pm}\frac{\alpha}{2}\tanh(|k|h)\right], \tag{29}$$

whose dimensionless form is written as

$$\mathcal{E} = \frac{\left[\tilde{\omega}^{\pm} - \kappa^{\pm}\mathrm{Fr}|\tilde{k}|\right]\left[\tilde{\omega}^{\pm} + \kappa^{\pm}\Omega\tanh|\tilde{k}|\right]}{|\tilde{k}|\tanh|\tilde{k}|}. \tag{30}$$

By analyzing Eq. (30), it is easily verified that the total energy may also be negative along with kinetic energy and that too only for counter-propagative waves, i.e., when $\tilde{\omega}^{-} + \mathrm{Fr}|\tilde{k}| > 0$ and $\tilde{\omega}^{-} - \Omega\tanh|\tilde{k}| < 0$, where $\tilde{k} < 0$. The first condition is valid for any negative $\tilde{k}$, whereas the second condition, with the help of the dispersion relation [Eq. (9)] for $\tilde{\omega}^{-}$, yields

$$-\mathrm{Fr}|\tilde{k}| + \sqrt{\left(\Omega\tanh|\tilde{k}|\right)^2 + \left(D\tilde{k}^4 - Q\tilde{k}^2 + 1\right)|\tilde{k}|\tanh|\tilde{k}|} < 0$$

$$\text{or } \mathrm{Fr} > \mathrm{Fr}_c = \sqrt{\left\{\left(1 - Q\tilde{k}^2 + D\tilde{k}^4\right) + \Omega^2\frac{\tanh|\tilde{k}|}{|\tilde{k}|}\right\}\frac{\tanh|\tilde{k}|}{|\tilde{k}|}}. \tag{31}$$

C. Blocking and buckling

Wave blocking is a particular phenomenon which occurs when a wave train encounters an opposing current. Due to the increasing opposing current, the wave train decelerates and, at a sufficiently strong current, the group velocity vanishes which results in wave blocking. In terms of wave energy, the total energy of the medium with the excited wave (NEW) becomes less than that without the wave. At the blocking point, other reflected waves are generated, and one of them contains negative energy. Hence, wave blocking, characterized by the vanishing of the group velocity of a wave train, initiates the process of NEW generation. A large number of scientific studies on the blocking phenomenon are already in existence in the literature. A similar phenomenon is also observed for flexural-gravity waves not only for propagation against an opposing current but also for sufficiently large compressive force (see Ref. 13). Consequently, the condition of wave blocking for counter-propagating waves ($\tilde{k} < 0$) is obtained by differentiating the dispersion relation (14) with respect to $\tilde{k}$ and setting $\frac{d\tilde{\omega}}{d\tilde{k}} = 0$ as

$$\left\{2\Omega^2\tanh\tilde{k} + \left(D\tilde{k}^4 - Q\tilde{k}^2 + 1\right)\tilde{k}\right\}\left(1 - \tanh^2\tilde{k}\right) + \left(5D\tilde{k}^4 - 3Q\tilde{k}^2 + 1\right)\tanh\tilde{k} + 2\left(\mathrm{Fr} - \Omega\mathrm{sech}^2\tilde{k}\right) \times \sqrt{\Omega^2\tanh^2\tilde{k} + \left(D\tilde{k}^4 - Q\tilde{k}^2 + 1\right)\tilde{k}\tanh\tilde{k}} = 0. \tag{32}$$

The above equation will be utilized to obtain the critical wavenumber ($\tilde{k}_b$) corresponding to wave blocking. Furthermore, by solving the same equation for Fr, it is possible to find the critical Froude number Fr_b for which a wave train having wavenumber $\tilde{k} < \tilde{k}_b$ will be blocked as

$$\mathrm{Fr}_b = \frac{1}{\cosh^2\tilde{k}_b}\left[\Omega - \frac{\left(2\left(D\tilde{k}_b^4 - Q\tilde{k}_b^2 + 1\right)\tilde{k}_b + 4\Omega^2\tanh\tilde{k}_b\right) + \left(5D\tilde{k}_b^4 - 3Q\tilde{k}_b^2 + 1\right)}{4\sqrt{\Omega^2\tanh^2\tilde{k}_b + \left(D\tilde{k}_b^4 - Q\tilde{k}_b^2 + 1\right)\tilde{k}_b\tanh\tilde{k}_b}}\right]. \tag{33}$$

Substituting Eq. (33) into the dispersion relation (14), the corresponding blocking frequency for the counter-propagating wave is obtained as

$$\tilde{\omega}_b = \left(\tanh\tilde{k}_b - \frac{\tilde{k}_b}{\cosh^2\tilde{k}_b}\right) + \left[\frac{2\Omega^2\tanh\tilde{k}_b + \tilde{k}_b}{2\sqrt{\Omega^2\tanh^2\tilde{k}_b + \left(D\tilde{k}_b^4 - Q\tilde{k}_b^2 + 1\right)\tilde{k}_b\tanh\tilde{k}_b}} - \Omega\right] + \frac{\left\{\left(Q\tilde{k}_b^2 - 3D\tilde{k}_b^4\right)\tanh\tilde{k}_b - \left(D\tilde{k}_b^5 - Q\tilde{k}_b^3\right)\mathrm{sech}^2\tilde{\mathrm{k}}_\mathrm{b}\right\}\tilde{k}_b}{2\sqrt{\Omega^2\tanh^2\tilde{k}_b + \left(D\tilde{k}_b^4 - Q\tilde{k}_b^2 + 1\right)\tilde{k}_b\tanh\tilde{k}_b}}. \tag{34}$$

Furthermore, with the help of the normalized wave period $\tilde{T}_b = T_b\sqrt{\frac{g}{h}}$, the dependency between the frequency of the blocked wave and the critical Froude number is represented as

$$\mathrm{Fr}_b = \mathrm{Fr}(\tilde{k}_b, \Omega, Q),\ \tilde{T}_b = \frac{2\pi}{\tilde{\omega}_b(\tilde{k}_b, \Omega, Q)}.$$

1. Flexural gravity wave blocking in deep water

Within the framework of the deep-water approximation, $|\tilde{k}| \gg 1$, the dispersion relation (14) for the counter-propagating wave is represented as

$$\tilde{\omega} = \left(\tilde{k}\mathrm{Fr} - \Omega\right) + \sqrt{\Omega^2 + \left(D\tilde{k}^4 - Q\tilde{k}^2 + 1\right)\tilde{k}}. \tag{35}$$

The condition for wave blocking $\left(\frac{d\tilde{\omega}}{d\tilde{k}} = 0\right)$ yields

$$\mathrm{Fr}_b = \frac{5D\tilde{k}_b^4 - 3Q\tilde{k}_b^2 + 1}{2\sqrt{\Omega^2 + (D\tilde{k}_b^4 - Q\tilde{k}_b^2 + 1)\tilde{k}}}. \tag{36}$$

The frequency of the blocked wave is obtained by substituting Fr_b in Eq. (35) as

$$\tilde{\omega} = \frac{-3D\tilde{k}_b^5 + Q\tilde{k}_b^3 + \tilde{k}_b + 2\Omega^2}{2\sqrt{\Omega^2 + \left(D\tilde{k}_b^4 - Q\tilde{k}_b^2 + 1\right)\tilde{k}_b}} - \Omega. \tag{37}$$

2. Flexural gravity wave blocking in shallow water

Another limiting case is the shallow water approximation $|\tilde{k}| \ll 1$. The dispersion relation, under the shallow water approximation, is obtained from Eq. (14) as

$$\tilde{\omega} = \left(\tilde{k}\mathrm{Fr} - \tilde{k}\Omega\right) + \tilde{k}\sqrt{\Omega^2 + \left(D\tilde{k}^4 - Q\tilde{k}^2 + 1\right)}. \tag{38}$$

The condition of wave blocking $\left(\frac{d\tilde{\omega}}{d\tilde{k}} = 0\right)$ yields

$$\mathrm{Fr}_b = \Omega + \frac{3D\tilde{k}_b^4 - 2Q\tilde{k}_b^2 + \Omega^2 + 1}{\sqrt{\Omega^2 + \left(D\tilde{k}_b^4 - Q\tilde{k}_b^2 + 1\right)}}. \tag{39}$$

Substituting Fr_b in Eq. (38), the following blocking frequency is obtained:

$$\tilde{\omega}_b = \frac{4D\tilde{k}_b^5 - 3Q\tilde{k}_b^3 + 2(\Omega^2+1)}{\sqrt{\Omega^2 + \left(D\tilde{k}_b^4 - Q\tilde{k}_b^2 + 1\right)}}. \tag{40}$$

III. NUMERICAL RESULTS

The effects of vorticity, Froude number, and compressive force on wave blocking and the occurrence of negative energy waves are graphically illustrated in this section. For numerical calculation, the following fixed parameter values are chosen: $EI = 10^5$ Pa, $\rho = 1025$ kg m^{-3}, $g = 9.81$ m s^{-2}, and $h = 20$ m unless otherwise mentioned. This gives a value of $D = 6.2157 \times 10^{-5}$.

A. Negative energy waves

The conditions for the occurrences of negative energy waves are pictorially depicted here with the help of energy–ratio curves. Different values of the Froude number (Fr), compressive forces (Q), and vorticity parameter (Ω) are utilized for graphical demonstration. Branches $1', 2', 3'$ and $1, 2, 3$ are represented by the energy ratio for co- and counter-propagating waves, respectively. Figure 1 illustrates the variation of the normalized total wave energy for different values of the Froude number. It is observed that with an increase in the Froude number, the total energy for counter-propagating waves decreases significantly and can even become negative (as seen for lines 3^- and 4^-). Hence, the increase in the current speed results in an increase in the absolute value of the negative kinetic energy, which, in turn, reduces the total energy even further to a negative value. However, this situation does not arise in the case of co-propagating waves and the total energy increases with an increase in Fr.

Figure 2 demonstrates the effect of the compressive force and vorticity on the total wave energy with Fr = 0.4. It is observed from Fig. 2(a) (pertaining to $\Omega = 0$) that the total energy becomes negative for a range of wavenumbers [the range (α, β) in line 3^- for example], which happens only for counter-propagating waves. This situation does not arise in the case of co-propagating waves (lines 1^+, 2^+, and 3^+). As the compressive force decreases from $2\sqrt{D}$, the aforementioned range also shrinks. This can be observed from the cut points of curves 1^- and 2^- with the horizontal axis. Hence, it can be concluded that the compressive force has a favorable impact on the generation of NEW for a counter-propagating wave. One surprising observation made is the vanishing of the total energy at point P which is due to the occurrence of wave buckling. In that situation, the plate breaks and both the kinetic and potential energies vanish to give zero total energy. On the other hand, the vanishing of the total energy at points α and β is different as kinetic and potential energies cancel each other and the vanishing is not due to wave buckling.

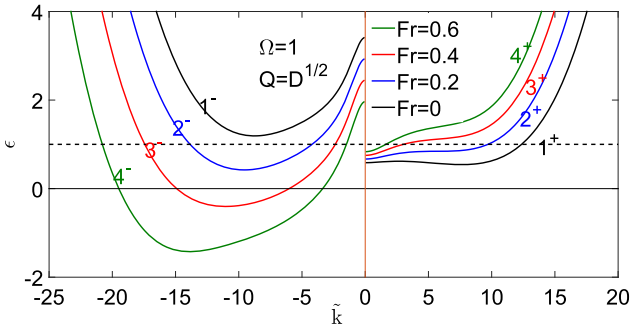

FIG. 1. Variation of the total wave energy for different values of Fr with $\Omega = 1$ and $Q = \sqrt{D}$. The occurrence of NEWs is observed for Fr = 0.4, 0.6 in the case of counter-propagating waves. NEW occurs within a range of wavenumbers which expands with an increase in current speed. Moreover, the absolute value of the negative wave energy increases with an introduction of higher current. However, the same does not occur for co-propagating waves.

Now, Fig. 2(b) deals with total wave energy for the same set of parameter values except for the vorticity which is 1. The pattern of the graphs is very similar to that observed in Fig. 2(a). However, one striking difference is obtained in terms of the vanishing of point P for line 3^-. Hence, the existence of vorticity prevents the buckling and, consequently, breaking of waves. In the case of co-propagating waves, the introduction of the vorticity increases the total positive energy further. Overall, it can be inferred that the effect of vorticity is very similar to that of Fr.

The variation of the energy ratio for different values of the compressive force is investigated in Fig. 3. Figure 3(a) pertains to the case when the flow is uniform, whereas the effect of vorticity is illustrated in Fig. 3(b). In the absence of vorticity, kinetic energy is always higher than potential energy for co-propagating waves. However, kinetic energy can become negative for counter-propagating waves within a range of wavenumbers. This situation is illustrated by lines 1^-, 2^-, and 3^- in Fig. 2(a), and (α, β) in line 3^- is one of such ranges. Outside such range, kinetic energy is always positive and less than potential energy. Moreover, the effect of the compressive force is mainly observed in that range where the energy ratio increases with an increase in the compressive force. When the buckling occurs for $Q = 2\sqrt{D}$, both the potential and kinetic energies vanish simultaneously, and consequently, the energy ratio blows up. This can be observed by line 3^-. However, the observations are a little bit different when the effect of vorticity is taken into account. The kinetic energy for co- and counter-propagating waves can become smaller and higher, respectively [Fig. 3(b)]. This is easily evident from arcs $A'B'$ and AB for co- and counter-propagating waves. Since the potential energy does not depend on flow vorticity, it vanishes at the same point, as observed in Fig. 3(a). However, the kinetic energy exists due to the vorticity. As a result, the energy ratio blows up (see line 3^-), but the corresponding total energy does not vanish [earlier observed in Fig. 2(b)].

Figure 4 depicts the dependency of the flexural rigidity, compressive force, and Froude number on NEW generation for both the cases of deep and shallow water approximations with zero vorticity. In the absence of the compressive force, the minimum Froude number for negative energy wave generation does not differ in both the cases [as observed in Fig. 4(a)] when the plate rigidity decreases. A significant difference is observed with a more rigid floating plate. Furthermore, a stronger current is required to excite NEW as the plate rigidity increases. On the other hand, the effect of the compressive force is illustrated in Fig. 4(b). For a plate with fixed flexural

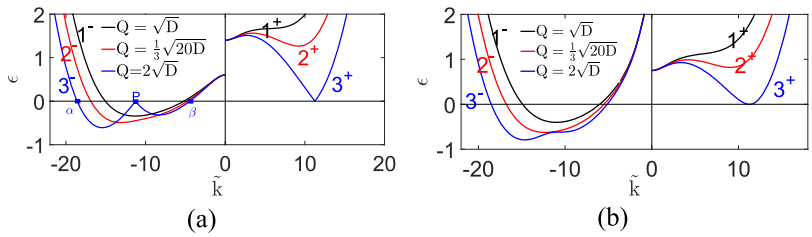

FIG. 2. Dimensionless total wave energy for different values of the compressive force is illustrated. (a) NEW exists for counter-propagating waves within a range of wavenumbers [(α, β) in the case $Q = 2\sqrt{D}$] and the range shrinks with a decrease in the compressive force. Higher compressive force contributes to the generation of NEW having a higher negative energy. Point P corresponds to the occurrence of buckling (breaking of the plate), and both the potential and kinetic energies vanish. At the point of breaking, both potential and kinetic energies become zero which results in $\epsilon = 0$, and it is equivalent to flexural gravity wave buckling. We can see from the figure that negative energy waves exist at both sides of the point P. However, the sudden vanishing of negative energy at P is possible due to wave buckling only. Otherwise, the curve would have been smooth. (b) Introduction of vorticity $\Omega = 1$ prevents the buckling and hence acts as a factor that negates the effect of the compressive force. (a) With vorticity $\Omega = 0$ and Fr = 0.4. (b) With vorticity $\Omega = 1$ and Fr = 0.4.

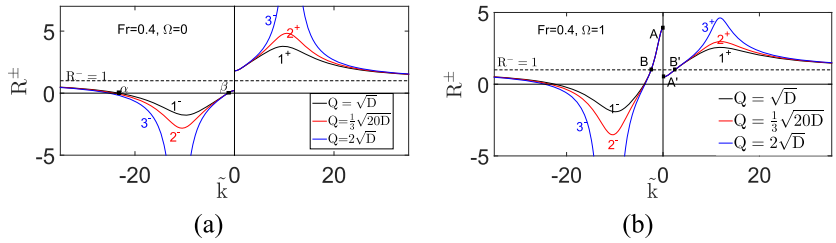

FIG. 3. Effect of the flow vorticity on the energy ratio is demonstrated for different values of the compressive force. (a) Kinetic energy is always higher than the potential energy for co-propagating waves with $\Omega = 0$. However, for counter-propagating waves, the kinetic energy can become negative within a certain range of wavenumbers [(α, β) for $Q = \sqrt{D}$]. A change in the energy ratio with respect to the compressive force is observed in a range of wavenumbers, and the kinetic energy is always less than the potential energy outside that range [beyond (α, β) for $Q = \sqrt{D}$]. The blow-up of the energy ratio for $Q = 2\sqrt{D}$ is due to the wave buckling which is observed earlier in Fig. 2(a). (b) With $\Omega = 1$, the kinetic energy can become higher than the potential energy for counter-propagating waves for range AB, and a reverse pattern can be observed for co-propagating waves for range $A'B'$. (a) With vorticity $\Omega = 0$ and Fr = 0.4. (b) With vorticity $\Omega = 1$ and $Fr = 0.4$.

rigidity, the compressive force accelerates the generation of NEW that can be identified by the decreasing nature of the curves. A lower Froude number is required as the compressive force acting on the plate increases. Interestingly, the deep water approximation matches exactly with the shallow water approximation.

The dependency between the critical Froude number to generate NEW and the corresponding wavenumber is shown in Fig. 5 for three different values of the compressive force both with and without vorticity. It is observed in both Figs. 5(a) and 5(b) that the range of wavenumbers in which NEW appears for a particular Froude number ($\mathrm{Fr}_c = 0.4$ in this case) widens with the increase in the compressive force irrespective of the vorticity. This can be observed from the wavenumber ranges (α_1, β_1) in line 1, (α_2, β_2) [see Fig. 5(a)] in line 2, and (α_3, β_3) in line 3 for the compressive forces $Q = \sqrt{D}$, $Q = \sqrt{20D}/3$, and $Q = 2\sqrt{D}$, respectively. A similar observation is made when the vorticity $\Omega = 1$ in Fig. 5(b). However, a higher Froude number is required to excite NEW in the presence of vorticity and this can be observed from the uplift of the curves. Furthermore, in the presence of vorticity, the occurrence of NEW starts with a relatively higher wavenumber for a fixed Froude number. This can be observed from the leftward shift of points α_1, α_2, and α_3 for $\mathrm{Fr}_c = 0.4$.

B. Wave blocking

The effect of dimensionless parameters such as the Froude number (Fr), vorticity (Ω), and compressive force (Q) on flexural gravity wave blocking is studied. The following notations

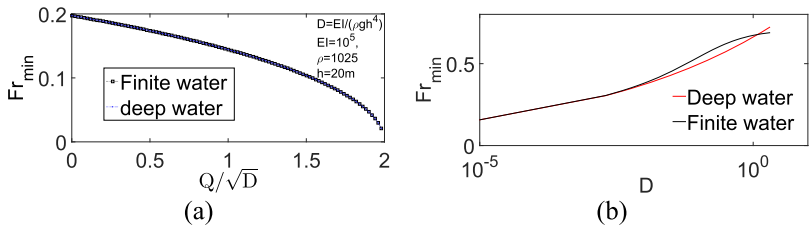

FIG. 4. The dependency of the flexural rigidity D and normalized compressive force $Q/\sqrt{D}$ on Fr_{min} for the existence of negative kinetic energy is plotted for finite depth and the deep water approximation. The vorticity is taken to be zero in both the cases. (a) In the absence of the compressive force, the deep water approximation matches with the finite depth results. This is observed in the portion when $D \to 0$. The difference is prominent when D takes higher values. The increasing nature of the graphs suggests that higher current speed is required to achieve negative kinetic energy when the floating plate becomes more rigid (higher values of D). (b) Deep-water approximation matches perfectly with the finite depth formulation when the compressive force changes, keeping D fixed. Interestingly, lower current speed contributes to the generation of negative kinetic energy when the compressive force increases. (a) $Q = 0$. (b) $D = EI/\rho g h^4$.

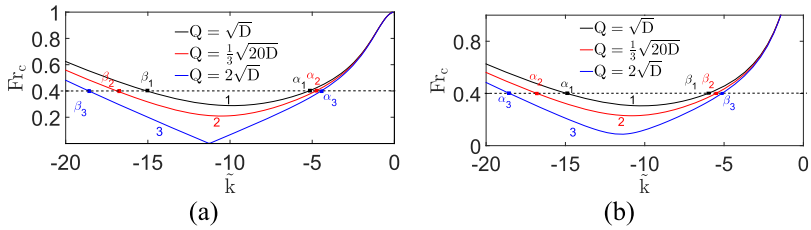

FIG. 5. Dependency of the critical Froude number Fr_c for the generation of NEW is studied for different values of the compressive force. (a) In the absence of vorticity, the horizontal dashed line cuts each of the curves in two distinct points, e.g., (α_1, β_1), (α_2, β_2), and (α_3, β_3), respectively, for lines 1, 2, and 3. Those points correspond to the terminal values of wavenumbers where NEW comes to existence for Fr = 0.4. NEW propagates in between those two wavenumbers for that specific Fr. The range of existence of NEW increases with an increase in the compressive force. (b) When vorticity is introduced, a higher Froude number is required to generate NEW. (a) $\Omega = 0$, $EI = 10^5$, $\rho = 1025$, $h = 20$. (b) $\Omega = 1$ $EI = 10^5$, $\rho = 1025$, $h = 20$.

are used to better illustrate the figures: Dispersion curves $\tilde{\omega}^{\pm}$ and corresponding phase speeds $\tilde{c}^{\pm}$ are represented by lines 1^+–3^+ for co-propagating waves, i.e., for $\tilde{k} > 0$ with κ^+, and 1^-–3^- for counter-propagating waves (for $\tilde{k} < 0$ with κ^-). $1_r^- - 3_r^-$ represent the counterparts for positive frequencies and wavenumbers.

Figure 6 describes the wave transformation of flexural gravity waves for different Froude numbers. For incoming waves with a fixed frequency $\tilde{\omega}_0$, line 1^- cuts the straight line $\tilde{\omega} = \tilde{\omega}_0$ at P which corresponds to an incident wave. Now, as the Froude number increases, the dispersion curve 1^- transforms to curve 2^-, and the incident wave is blocked at point B_1 due to the occurrence of a maximum where the group velocity vanishes. Now at this point, the blocked wave is transformed into other waves which propagate away from the blocking point. One of the reflected waves lies on that same branch but on the left side of the maximum along the negative slope of the curve (along B_1B_2). This wave has a smaller wavelength than the incident wave, a negative phase speed but a positive group velocity, and consequently the energy flux is in

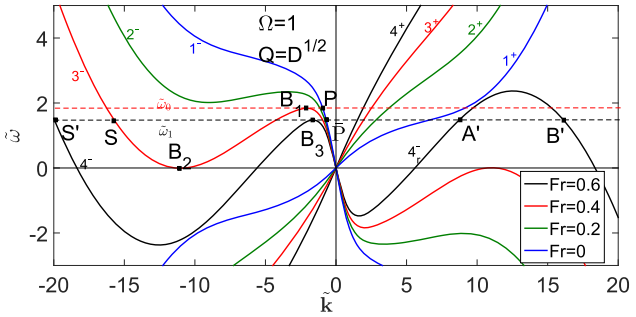

FIG. 6. Transformation of a flexural gravity wave at the blocking point due to a change in the Froude number is illustrated. For an incoming wave of fixed frequency $\tilde{\omega}_0$, point P corresponding to the incident wavenumber transforms to blocking point B_1 with the increase in the current, as curve 1^- transforms to curve 3^-. After that, the wave transforms into two reflected waves, one along B_1B_2 and another corresponding to P', and one transmitted wave corresponding to S. Waves corresponding to P' and S do not encounter blocking as they travel toward $+\infty$ and $-\infty$, respectively. But, the wave along B_1B_2 achieve one minimum at B_2, hence encountering blocking. Since this wave travels with the current, its wavenumber will increase and the graph will change adiabatically to have the blocking point B_2 at the frequency $\tilde{\omega}_0$. This point is the secondary blocking at the same frequency. Similarly, for fixed incoming frequency $\tilde{\omega}_1$ with the wavenumber corresponding to $\bar{P}$, five waves are generated from the blocking observed at B_3 such as waves corresponding to points S', A', B', $\bar{P}$ (after adiabatic change in the graph) and one wave in branch 4^+ with frequency $\tilde{\omega}_0$. Out of these, A' (positive group velocity) and B' (negative group velocity) are the negative energy waves.

the direction of the current. When this wave propagates along with the current, its wavenumber (absolute value) increases. Another reflected wave propagates along with the current with positive phase and group velocities (point P' corresponds to such a wave). Lastly, one transmitted wave is generated with a sufficiently large wavenumber (corresponding to point S in the negative branch). This wave has a negative phase and group velocity and propagates against the current. Now the waves corresponding to points P' and S do not encounter blocking any further as they propagate toward $+\infty$ and $-\infty$, respectively. But the wave which travels along B_1B_2 encounters a minimum B_2. Now when this wave travels with the current, the graph also changes (adiabatic change) and the corresponding minimum B_2 will occur eventually at frequency $\tilde{\omega}_0$. It is to be noted that as the graph changes, point B_2 shifts its position. This blocking point is called the secondary blocking point at which other waves are generated. As observed in the case of a primary blocking point, there are two reflected waves in the same branch (negative branch) of the dispersion graph with negative phase speeds and group velocities but different wavenumbers (points correspond to P after an adiabatic change and S). Apart from this, one transmitted wave in the positive branch is also generated having positive phase speed and group velocity. This wave and the reflected wave with a higher wavenumber propagate toward $+\infty$ and $-\infty$, respectively, and the reflected wave with a smaller wavenumber propagates against the current and again goes through the primary blocking. This process of wave transformation is repeated several times.

Hence, we get two blocking points which are spatially separated, and the incident waves are locked therein. However, at each reflection from the blocking point, the wave energy is dissipated via transmitted waves. A similar observation was made earlier by Maïssa, Rousseaux, and Stepanyants[8] for gravity wave propagation in the presence of surface tension, and the subsequent transformation from gravity to capillary-gravity waves was established.

Another special type of flexural-gravity wave is observed when at the blocking point the incident wave transforms into waves that contain negative energy waves. This observation is also illustrated in Fig. 6. Consider a wave train of frequency $\tilde{\omega}_1$. The incident wave is characterized by point $\bar{P}$ where line $\tilde{\omega} = \tilde{\omega}_1$ cuts dispersion graph 1^-. As the current speed increases, the wavenumber of the incident wave increases and is eventually blocked at point B_3. It is to be noted that the portion of curve 4^- which has a negative frequency is equivalent to curve 4_r^+ with a positive frequency. Subsequently, the

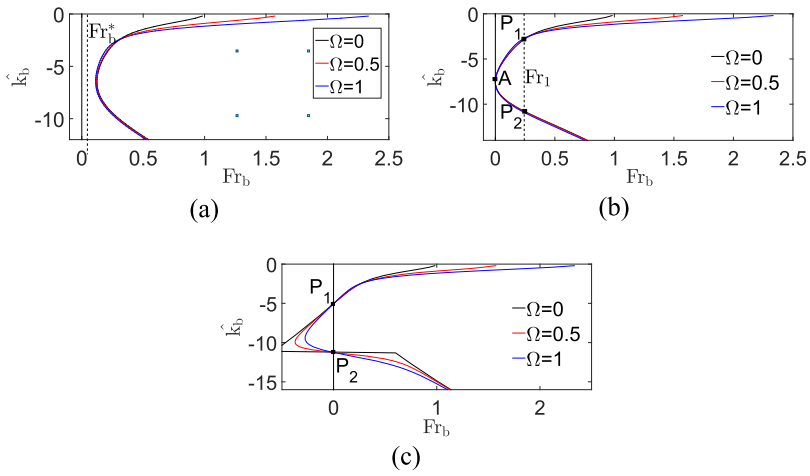

FIG. 7. Dependency of the Froude number Fr_c against the blocked wavenumber is studied for different values of the flow vorticity and compressive force. (a) When $Q = \sqrt{D}$, the opposing current is required to block the wave. Fr_b^* denotes the minimum Froude number to achieve wave blocking, and the flow vorticity has a negligible effect on Fr_b^*. However, for relatively longer waves, i.e., k_b is small, a higher Froude number is required to block the wave when the flow vorticity is high. (b) When $Q = \frac{1}{3}\sqrt{20D}$, wave blocking is achieved even with Fr = 0. Point A corresponds to the blocked wavenumber related to such an occurrence. This phenomenon is equivalent to the occurrence of a point of inflexion in the dispersion curve as seen in the work of Das, Sahoo, and Meylan.[13] Also, there exist two blocked wavenumbers for a particular Fr (points P_1 and P_2 pertaining to Fr_1 are basically primary and secondary blocking points, respectively). (c) In the case of $Q = 2\sqrt{D}$, the discontinuity for the black curve is due to the occurrence of buckling which ceases to exist when the flow vorticity is introduced (as the graphs are smooth for non-zero vorticity). Occurrences of the primary and secondary blocking exist even when Fr = 0 (corresponding to points P_1 and P_2). (a) $Q = \sqrt{D}$, (b) $Q = \frac{1}{3}\sqrt{20D}$, (c) $Q = 2\sqrt{D}$.

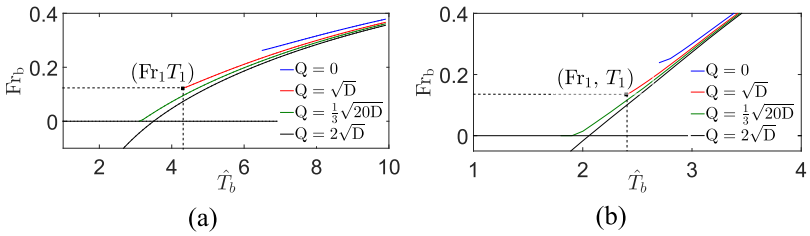

FIG. 8. The dependency between the Froude number and the period of blocked (primary) waves is illustrated for different values of the compressive force acting on the plate. (a) Non-existence of the curves below a specific value of $(\mathrm{Fr}_b, \hat{T}_b)$ suggests a minimum value of Fr and $\hat{T}$ to initiate primary blocking [e.g., (Fr_1, T_1) in the red curve corresponding to $Q = \sqrt{D}$]. Moreover, in the absence of the compressive force, the primary blocking gets initiated at a higher period and Froude number (blue curve), and with an increase in the compressive force, the corresponding values decreases. (b) With the introduction of vorticity, a significant change is observed in the values of (Fr_1, T_1). Interestingly, the primary blocking is observed even in the absence of the current as seen from the cut points of curves with line $\mathrm{Fr}_b = 0$ in both the figures. (a) $\Omega = 0$. (b) $\Omega = 1$.

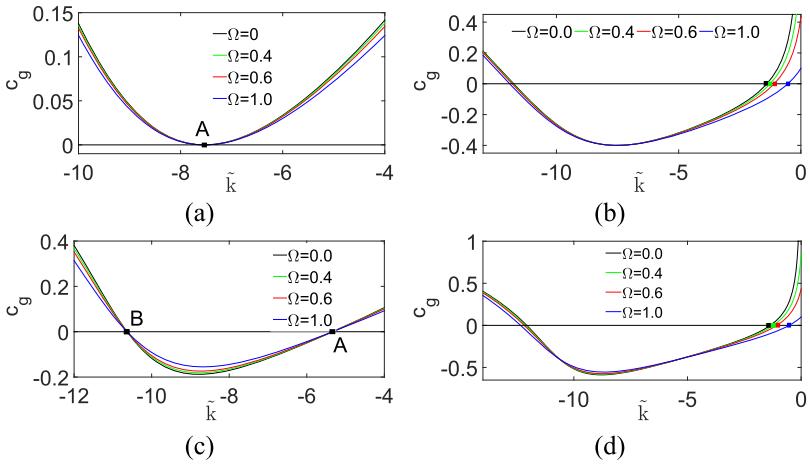

FIG. 9. Variation of the group velocity which characterizes the rate of wave energy propagation is studied against the dimensionless wavenumber for different values of vorticity. (a) In the absence of the current (Fr = 0) and $Q = \sqrt{20D}/3$, the group velocity vanishes at the wavenumber denoted by point A, irrespective of the vorticity value. This corresponds to the point of inflexion as described in the work of Das, Sahoo, and Meylan.[13] (b) With the introduction of current, the point of inflexion bifurcates to provide primary (denoted by colored dots) and secondary blocking points. In between these two blocking points, the wave energy will propagate in the opposite direction to the wave propagation. (c) However, in the absence of current, an increase in the compressive force ($Q = 1.86\sqrt{D}$) also bifurcates the point of inflexion into two blocking points. However, unlike in (b), the wavenumber corresponding to primary and secondary blocking is invariant under the effect of vorticity. (d) In the presence of both current and higher compressive force, the pattern of the graph is similar to that obtained in (b) but with an increase in the rate of energy propagation in the opposite direction. (a) Fr = 0 and $Q = \sqrt{20D}/3$. (b) Fr = 0.4 and $Q = \sqrt{20D}/3$. (c) Fr = 0 and $Q = 1.86\sqrt{D}$. (d) Fr = 0.4 and $Q = 1.86\sqrt{D}$.

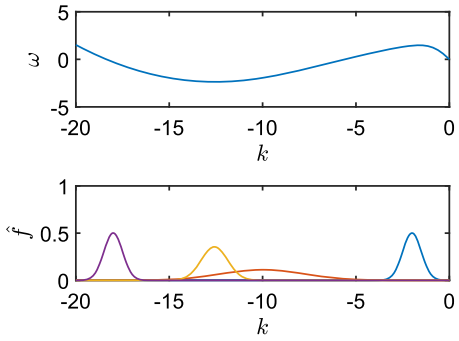

FIG. 10. The dispersion equation for the case we consider in Figs. 11–14 (Multimedia view) is shown in the top figure. In the bottom figure, $|\hat{f}|$ is plotted for $\tilde{k}_c = -2$ and b = 2, the values used in Fig. 11 (Multimedia view) in the blue curve. The red curve corresponds to $\tilde{k}_c = -10$ and b = 0.1 [values for Fig. 12 (Multimedia view)], the yellow curve corresponds to $\tilde{k}_c = -12.58$ and b = 2 [values for Fig. 13 (Multimedia view)], and the purple curve corresponds to $\tilde{k}_c = -18$ and b = 2 [values for Fig. 14 (Multimedia view)].

maximum in curve 4^- occurs at a lower frequency than that of 4_r^+. At this blocking point, the incident wave transforms into five waves. First, there is a wave with a higher wavenumber (absolute value) and negative phase but positive group velocity that travels along with the current. There are two reflected waves, one with a large wavenumber (absolute) and negative phase speed but positive group velocity in the same branch and another with a comparatively smaller wavenumber and positive phase and group velocities in branch 4^+. These two waves propagate toward $-\infty$ and ∞, respectively. All these three waves have positive energy. Interestingly, there exist two more waves with positive phase speeds in branch 4_r^-, one of which has a positive group velocity (corresponding to A'), while the other has a negative group velocity (corresponding to B'). These two waves are actually negative energy waves and are not observed in the discussion of preceding paragraphs.

A secondary wave blocking can also occur in this situation. The reflected wave occurring in branch 4^- (along the positive slope of the curve) propagates with the current, and consequently the dispersion graph changes to finally attain a minimum at the frequency $\tilde{\omega}_1$. Hence, the wave gets blocked and transforms into other waves as discussed earlier in the case of secondary blocking.

However, in this particular case, one of the negative energy waves (corresponding to A') co-propagates with the current and gets blocked at the maximum of the transformed curve 4_r^- (secondary blocking) at the frequency $\tilde{\omega}_1$. Transformation of the negative energy wave at the blocking point is difficult to determine.

Figure 7 demonstrates the dependency of the Froude number Fr_c against the blocked wavenumber k_b for different values of the flow vorticity and compressive force. Figure 7(a)

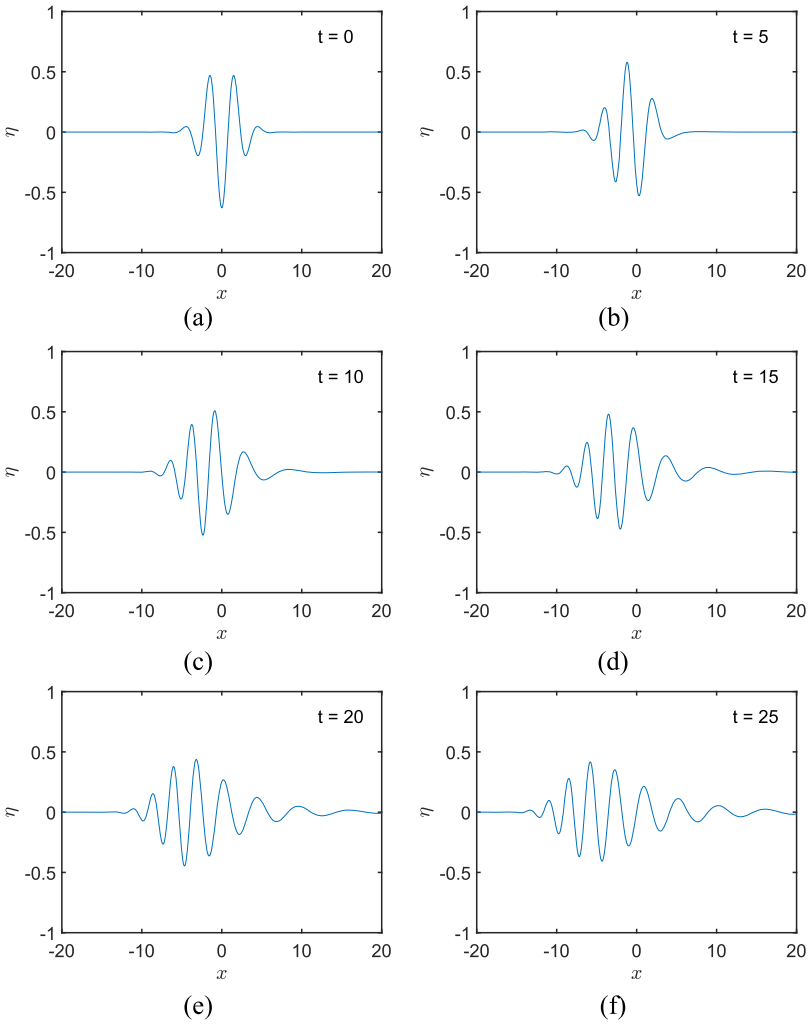

FIG. 11. The evolution of a Gaussian pulse given by Eq. (42) with $\tilde{k}_c = -2$ and b = 2 (which corresponds to the blue curve in Fig. 10) for the times shown. The standard D value is used, $Q = \sqrt{D}$, Fr = 0.6, and $\Omega = 1$. The evolution is also shown as an animation in the multimedia file (movie 1). (a) $t = 0$, (b) $t = 5$, (c) $t = 10$, (d) $t = 15$, (e) $t = 20$, (f) $t = 25$. Multimedia view: https://doi.org/10.1063/1.5052228.1

illustrates that an opposing current is required to block the incoming waves when $Q = \sqrt{D}$. Fr_b^* denotes the minimum Froude number required to achieve wave blocking. Moreover, flow vorticity has a negligible effect on Fr_b^* as it hardly shifts the minimum of the graph. However, a higher Froude number is required to block the wave when flow vorticity is high when the incoming waves have a relatively longer wavelength, i.e., k_b is small. On the other hand, wave blocking is achieved even with Fr = 0 when $Q = \frac{1}{3}\sqrt{20D}$. This observation can be realized from Fig. 7(b) where point A corresponds to the wavenumber of such a blocked wave. In fact, this point corresponds to the point of inflexion where wave blocking gets initiated which can be verified from the dispersion curve provided in the work of Das, Sahoo, and Meylan.[13] Furthermore, for a fixed Froude number of the flow [Fr_1, for example, as seen in Fig. 7(b)], there exist two blocked wavenumbers corresponding to points P_1 (primary blocking) and P_2 (secondary blocking). Finally, for $Q = 2\sqrt{D}$, wave buckling is observed from the discontinuity in the black curve in Fig. 7(c) when flow vorticity is absent. In terms of free-surface gravity waves, this kind of situation arises when the surface wave breaks. The kinematic criterion for such breaking was recently validated by Khait and Shemer[33] using fully non-linear numerical simulation with the help of the Boundary Element Method (BEM) followed by experiments. However, the buckling vanishes with the introduction of flow vorticity which is clearly visible from the smoothness of the red and blue curves. Moreover, the primary and secondary blocking occurs even when Fr = 0 for wavenumbers corresponding to points P_1 and P_2.

Figure 8 depicts the dependencies of the Froude number and period of the blocked waves for different values of the compressive force both in the presence and absence of flow vorticity. In both the figures, the dependency curve starts from a specific value of Fr_b and $\hat{T}_b$, namely, point (Fr_1, T_1) in the red curves of Figs. 8(a) and 8(b) for $Q = \sqrt{D}$ and $\Omega = 0$. This point suggests the initiation of blocking, known as the point of inflexion. Consequently, for any value of $\mathrm{Fr}_b < \mathrm{Fr}_1$ or $\hat{T}_b < \hat{T}_1$, blocking will never initiate. Moreover, the cut points of the curves corresponding to $Q = \sqrt{20D}/3$ and $Q = 2\sqrt{D}$ with $\mathrm{Fr}_b = 0$ ensure the occurrence of blocking in the absence of an opposing current. For a fixed value of vorticity, an increase in vorticity results in the appearance of blocking at lower values of the Froude number and period of the waves. Comparison of Fig. 8(b) with Fig. 8(a) reveals that, for a fixed value of the compressive force, flow vorticity prompts wave-blocking at a lower Froude number as well as period.

Now, the effect of the flow vorticity on the group velocity, which characterizes the rate of energy propagation, is studied in Fig. 9 for different values of the Froude number and

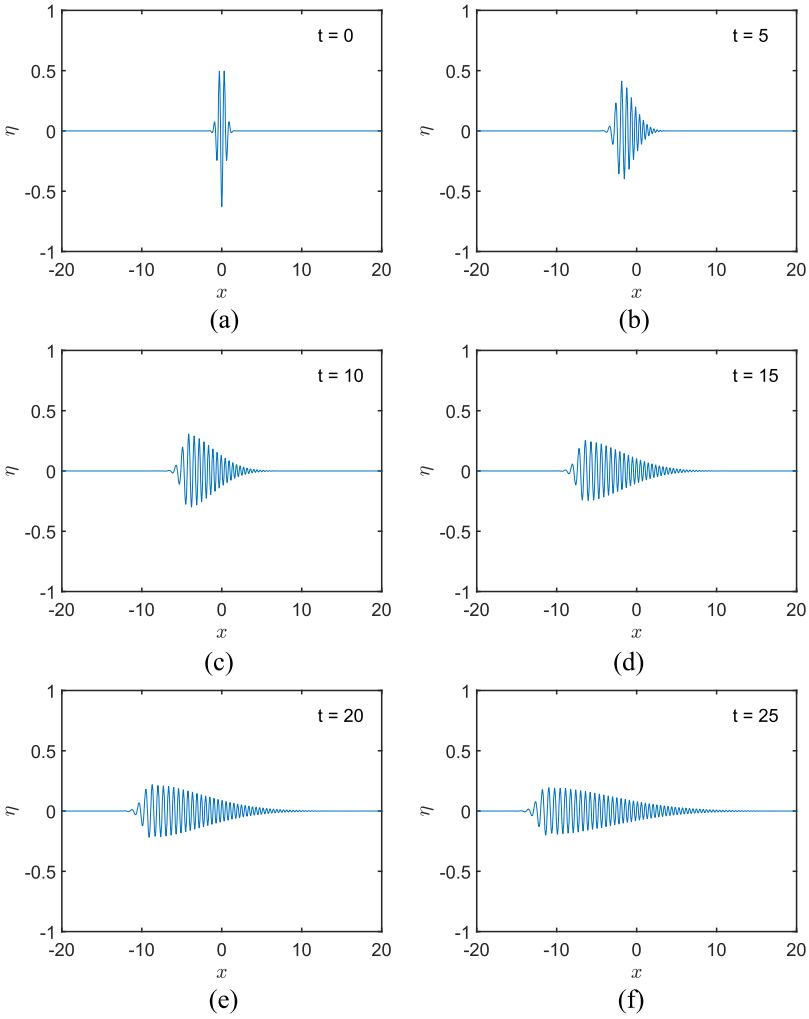

FIG. 12. As in Fig. 11 (Multimedia view) except with $\tilde{k}_c = -10$ and b = 0.1 (which corresponds to the red curve in Fig. 10). The evolution is also shown as an animation in the multimedia file (movie 2). (a) $t = 0$, (b) $t = 5$, (c) $t = 10$, (d) $t = 15$, (e) $t = 20$, (f) $t = 25$. Multimedia view: https://doi.org/10.1063/1.5052228.2

compressive force. The value of the wavenumber for which c_g becomes zero is pointed by A in Fig. 9(a) for Fr = 0 and $Q = \sqrt{20D}/3$. This corresponds to the point of inflexion (see Ref. 13) when blocking is initiated. Interestingly, the wavenumber corresponding to A is invariant under vorticity when Fr = 0. However, with the introduction of current (Fr = 0.4), point A bifurcates into two different blocking points (two different cut points for each of the curves with line $c_g = 0$), as observed in Fig. 9(b). But the invariance in the blocked wavenumber is lost [four colored dots in Fig. 9(b)] due to the introduction of current. However, in the absence of current, higher values of the compressive force [$Q = 1.86\sqrt{D}$ as in Fig. 9(c)] also bifurcate the point of inflexion into two blocking points A (primary) and B (secondary) but preserving the invariance under vorticity. Moreover, comparison of Fig. 9(d) with Fig. 9(b) reveals an increase in the magnitude of c_g with the introduction of current and higher compressive force.

IV. TIME–DOMAIN SIMULATION

We present here the simulations of pulses in the time-domain. The plate surface motion is given by

$$\eta(x,t) = \mathrm{Re}\left\{\int_{-\infty}^{\infty} \hat{f}(\tilde{k}) \exp\left(\mathrm{i}\tilde{k} + \tilde{\omega}(\tilde{k})t\right)\mathrm{d}\tilde{k}\right\}. \tag{41}$$

Note that we only consider values of $\hat{f}(\tilde{k})$ which are non-zero for $\tilde{k} < 0$. We consider the initial condition given by a Gaussian wave packet which we write in the transform space as

$$\hat{f}(\tilde{k}) = 2A\sqrt{\pi b}\exp\left(-b(\tilde{k} - \tilde{k}_c)^2\right), \tag{42}$$

where $\tilde{k}_c$ is the centre frequency, $A = 0.1$ is an amplitude function, and b is a spreading function.

We consider only a single value for the non-dimensional parameters, with D as before, $Q = \sqrt{D}$, Fr = 0.6, and $\Omega = 1$. The dispersion equation for this case is the black curve 4^- shown in Fig. 6. We consider four cases, in the first case, $\tilde{k}_c = -2$ and b = 2. The dispersion curve is shown in Fig. 10 and the absolute value of $\hat{f}(\tilde{k})$ for this case. For this example, the pulse is concentrated in waves with small wavelengths around a maximum in ω where ω is positive. Snapshots of this motion are shown in Fig. 11 (Multimedia view), while a movie of this is given in the multimedia file as movie 1. The phase velocity of the pulse will be to the right, while the pulse will spread very slowly with most of the energy remaining at $x = 0$ even after a long time. The short wavelength waves will have a small positive group velocity and can be seen moving to the left, while the long wavelength waves will have a small negative group velocity and can be seen moving to the right.

Figure 12 (Multimedia view) is the same computation as in Fig. 11 (Multimedia view) except that $\tilde{k}_c = -10$ and b = 0.1,

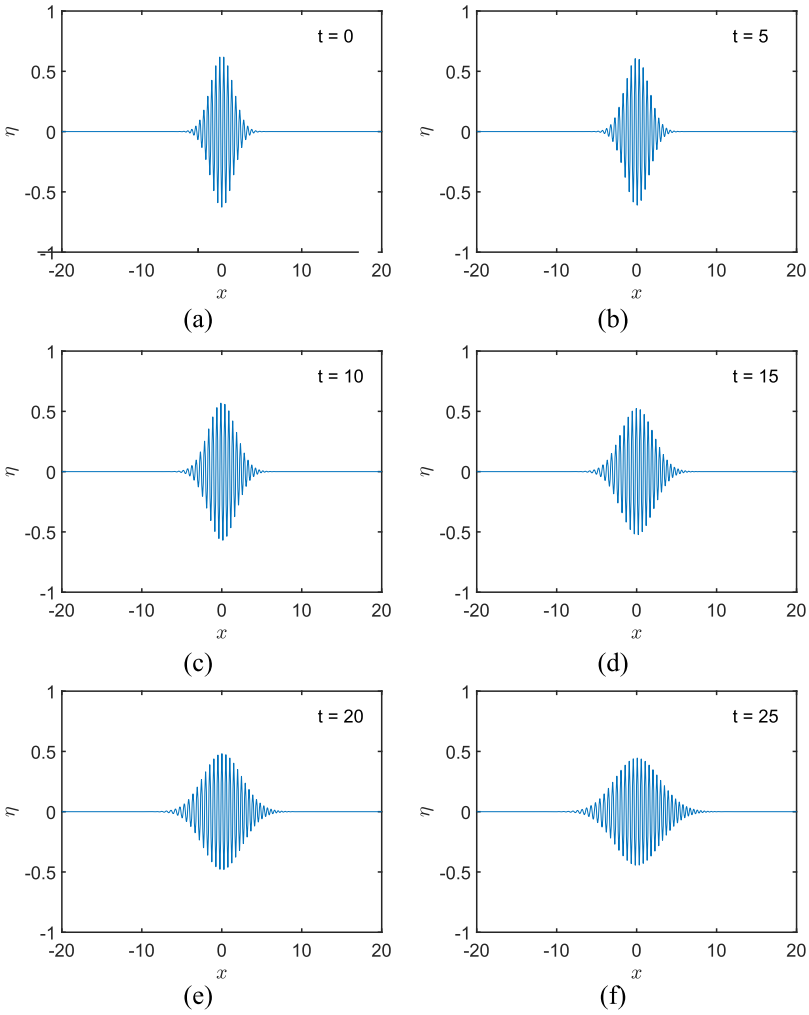

FIG. 13. As in Fig. 11 (Multimedia view) except with $\tilde{k}_c = -12.58$ and b = 2 (which corresponds to the yellow curve in Fig. 10). The evolution is also shown as an animation in the multimedia file (movie 3). (a) $t = 0$, (b) $t = 5$, (c) $t = 10$, (d) $t = 15$, (e) $t = 20$, (f) $t = 25$. Multimedia view: https://doi.org/10.1063/1.5052228.3

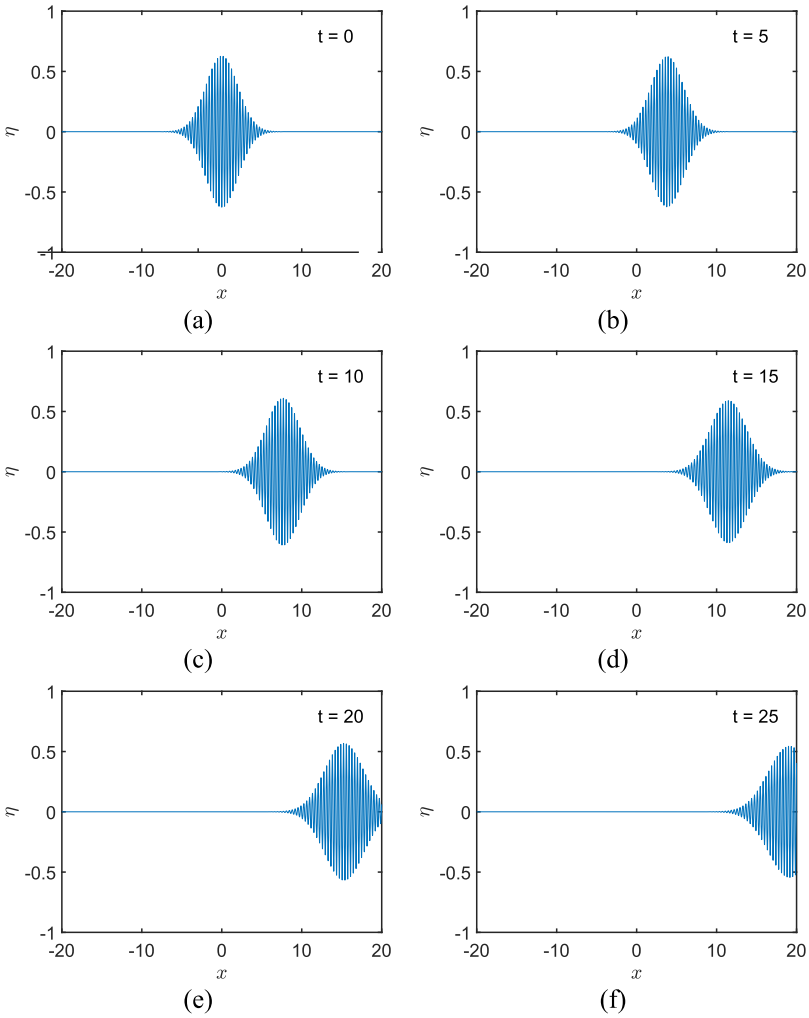

FIG. 14. As in Fig. 11 (Multimedia view) except with $\tilde{k}_c = -18$ and b = 2 (which corresponds to the purple curve in Fig. 10). The evolution is also shown as an animation in the multimedia file (movie 4). (a) $t = 0$, (b) $t = 5$, (c) $t = 10$, (d) $t = 15$, (e) $t = 20$, (f) $t = 25$. Multimedia view: https://doi.org/10.1063/1.5052228.4

values which correspond to the red curve in the lower figure of Fig. 10. In this case, the Gaussian pulse is highly concentrated at $t = 0$ but has a wide spread in the wavenumber space. Therefore the initial pulse spreads rapidly with the long wavelength spreading to the left and the short waves to the right, but the spreading is slow around the point of zero group velocity at approximately $\omega = -12.58$. Movie 2 in the multimedia file shows an animation of this motion. In Fig. 13 (Multimedia view), $\tilde{k}_c = -12.58$ and b = 2, which corresponds to the yellow curve in Fig. 10, so we concentrate around the zero in the group velocity. For this example, the pulse spreads very slowly without any motion. It is shown as an animation in movie 3 in the multimedia file. For Fig. 14 (Multimedia view), $\tilde{k}_c = -18$ and b = 2, which corresponds to the purple curve in Fig. 10 and the pulse simply moves to the right. The phase velocity is to the left which can be seen in movie 4 in the multimedia file. For experimental validation of the results, sophisticated measuring techniques are required in a controlled lab environment. Zavadsky, Benetazzo, and Shemer[34] recently applied independent measuring techniques, namely, 3D reconstruction of a stereo video image and 2D laser slope gauge, to measure spatial and temporal movements of surface gravity wave elevation and instantaneous surface slope direction, which leaves a scope to experimentally validate some of the results presented here.

V. CONCLUSION

The effects of the vorticity, compressive force, and Froude number on the occurrence of flexural-gravity wave blocking and generation of NEW are investigated with the help of linearized water wave theory and small amplitude structural response. Analytic forms for the threshold of NEW generation as well as blocking are established, and their dependencies with respect to different parameters such as vorticity, compressive force, Froude number are demonstrated graphically. In the absence of vorticity, kinetic energy is always higher than potential energy for co-propagating waves, while kinetic energy can become less than potential energy with the introduction of vorticity. In the case of counter-propagating waves, NEW propagates within a range of wavenumbers, and outside that range, kinetic energy is always less than potential energy. However, with the introduction of current, kinetic energy can become higher than potential energy. Moreover, the total wave energy can become negative in a specific wavenumber range with the proper choice of flow parameters. However, the total wave energy is always positive for co-propagating waves irrespective of parameter values. It is observed that the wavenumber corresponding to the point of inflexion and primary and secondary blocking is invariant under vorticity, whereas the period for the same shortens with an increase in vorticity.

ACKNOWLEDGMENTS

S.D. acknowledges IIT Kharagpur, INDIA, for the support as Post-Doctoral Fellowship when the work was initiated and the support received from SRM University AP–Amaravati, INDIA, as a faculty during which a part of the research work was pursued. T.S. acknowledges the Department of Science and Technology, Government of India, for the partial support through Grant No. DST/CCP/CoE/79/2017(G). M.H.M. acknowledges the Indian Institute of Technology Kharagpur for inviting to offer a short-term course (Course Id. 16IWT10) under Global Initiative of Academic Networks (GIAN) at IIT Kharagpur that initiated the collaborative work. M.H.M. also acknowledges Isaac Newton Institute for Mathematical Sciences for support and hospitality during the programme Mathematics of Sea Ice Phenomena when part of the work on this paper was undertaken. This work was supported by EPSRC Grant No. EP/K032208/1 and was also partially supported by a grant from the Simons Foundation. M.H.M. also thanks Clare Hall, Cambridge University, for the assistance of a visiting fellowship. This material is based upon research supported by, or in part by, the U.S. Office of Naval Research under Award No. N0001415-12611. The ARC Training Centre for Advanced Technologies in Rail Track Infrastructure also supported M.H.M. and S.D. (ARC IC17010006).

[1]L. C. Van Rijn, "Unified view of sediment transport by currents and waves. I: Initiation of motion, bed roughness, and bed-load transport," J. Hydraul. Eng. **133**, 649 (2007).
[2]I. Lavrenov, "The wave energy concentration at the Agulhas current off South Africa," Nat. Hazards **17**, 117 (1998).
[3]B. C. Gerwick, Jr., *Construction of Marine and Offshore Structures* (CRC Press, Boca Raton, FL, 2007).
[4]A. Chawla and J. T. Kirby, "Experimental study of wave breaking and blocking on opposing currents," Coastal Eng. **1998**, 759–772 (1999).
[5]I. Brevik, "The stopping of linear gravity waves in currents of uniform vorticity," Phys. Norv. **8**, 157 (1976).
[6]T. B. Benjamin, "The threefold classification of unstable disturbances in flexible surfaces bounding inviscid flows," J. Fluid Mech. **16**, 436 (1963).
[7]L. Ostrovskiĭ, S. A. Rybak, and L. S. Tsimring, "Negative energy waves in hydrodynamics," Sov. Phys.-Usp. **29**, 1040 (1986).
[8]P. Maïssa, G. Rousseaux, and Y. Stepanyants, "Negative energy waves in a shear flow with a linear profile," Eur. J. Mech.- B/Fluids **56**, 192 (2016).
[9]B. Kadomtsev, A. Mikhailovskii, and A. Timofeev, "Negative energy waves in dispersive media," J. Exp. Theor. Phys. **20**, 2266 (1964).
[10]M. V. Nezlin, "Negative-energy waves and the anomalous Doppler effect," Sov. Phys.-Usp. **19**, 946 (1976).
[11]R. Cairns, "The role of negative energy waves in some instabilities of parallel flows," J. Fluid Mech. **92**, 1 (1979).
[12]S. Å. Ellingsen and I. Brevik, "How linear surface waves are affected by a current with constant vorticity," Eur. J. Phys. **35**, 025005 (2014).
[13]S. Das, T. Sahoo, and M. H. Meylan, "Dynamics of Flexural Gravity Waves: From sea ice to Hawking radiation and analogue gravity," Proc. R. Soc. A **474**, 20170223 (2018).
[14]S. Das, T. Sahoo, and M. H. Meylan, "Flexural-gravity wave dynamics in two-layer fluid: Blocking and dead water analogue," J. Fluid Mech. **854**, 121 (2018).
[15]G. Taylor, "The action of a surface current used as a breakwater," Proc. R. Roc. A **231**, 466 (1955).
[16]R. Smith, "The reflection of short gravity waves on a non-uniform current," Math. Proc. Cambridge Philos. Soc. **78**, 517 (1975).
[17]D. Peregrine, "Interaction of water waves and currents," Adv. Appl. Mech. **16**, 9 (1976).
[18]R. A. Dalrymple, "A finite amplitude wave on a linear shear current," J. Geophys. Res. **79**, 4498, https://doi.org/10.1029/jc079i030p04498 (1974).
[19]J. T. Kirby and T.-M. Chen, "Surface waves on vertically sheared flows: Approximate dispersion relations," J. Geophys. Res. **94**, 1013, https://doi.org/10.1029/jc094ic01p01013 (1989).
[20]H. Nepf and S. G. Monismith, "Wave dispersion on a sheared current," Appl. Ocean Res. **16**, 313 (1994).
[21]J. W. Miles, "The hydrodynamic stability of a thin film of liquid in uniform shearing motion," J. Fluid Mech. **8**, 593 (1960).
[22]K. Trulsen and C. C. Mei, "Double reflection of capillary/gravity waves by a non-uniform current: A boundary-layer theory," J. Fluid Mech. **251**, 239 (1993).
[23]P. Maissa, G. Rousseaux, and Y. Stepanyants, in *Proceedings of the International Coastal Dynamics Conference* (Bordeaux University-SHOM, Arcachon, France, 2013).
[24]P. Maïssa, G. Rousseaux, and Y. Stepanyants, "Wave blocking phenomenon of surface waves on a shear flow with a constant vorticity," Phys. Fluids **28**, 032102 (2016).
[25]S. Tsao, "Behaviour of surface waves on a linearly varying flow," Tr., Mosk. Fiz.-Tekh. Inst. Issled. Mekh. Prikl. Mat. **3**, 66 (1959).
[26]D. Kheisin, "Nonstationary problem of the oscillations of an infinite elastic plate floating on the surface of an ideal liquid," Izv. Akad. Nauk SSSR, Mekh. Mashinostr. **1** (1962).
[27]D. Kheisin, "Dynamics of the ice cover," Technical Report AD0695178, Army Foreign Science and Technology Center, Washington, D.C., 1969.
[28]A. E. Bukatov, "Influence of a longitudinally compressed elastic plate on the nonstationary wave motion of a homogeneous liquid," Fluid Dyn. **15**, 687 (1980).
[29]E. B. Magrab and A. A. Leissa, "Vibrations of elastic structural members," J. Appl. Mech. **47**, 693 (1980).
[30]A. D. Kerr, "The critical velocities of a load moving on a floating ice plate that is subjected to in-plane forces," Cold Reg. Sci. Technol. **6**, 267 (1983).
[31]T. Sahoo, *Mathematical Techniques for Wave Interaction with Flexible Structures* (CRC Press, Boca Raton, FL, 2012).
[32]Y. A. Stepanyants and A. Fabrikant, "Propagation of waves in hydrodynamic shear flows," Sov. Phys.-Usp. **32**, 783 (1989).
[33]A. Khait and L. Shemer, "On the kinematic criterion for the inception of breaking in surface gravity waves: Fully nonlinear numerical simulations and experimental verification," Phys. Fluids **30**, 057103 (2018).
[34]A. Zavadsky, A. Benetazzo, and L. Shemer, "On the two-dimensional structure of short gravity waves in a wind wave tank," Phys. Fluids **29**, 016601 (2017).